IEEE Access
Multidisciplinary | Rapid Review | Open Access Journal

Received May 21, 2020, accepted July 3, 2020, date of publication July 14, 2020, date of current version July 23, 2020.

Digital Object Identifier 10.1109/ACCESS.2020.3009181

Identification of Communication Signals Using Learning Approaches for Cognitive Radio Applications

ZHENGJIA XU, (Graduate Student Member, IEEE), IVAN PETRUNIN, (Member, IEEE), AND ANTONIOS TSOURDOS, (Member, IEEE)
School of Aerospace, Transport and Manufacturing (SATM), Cranfield University, Cranfield MK43 0AL, U.K.
Corresponding author: Zhengjia Xu (zhengjia.xu@cranfield.ac.uk)

ABSTRACT Signal detection, identification, and characterization are among the major challenges in aerial communication systems. The ability to detect and recognize signals using cognitive technologies is still under active development when addressing uncertainties regarding signal parameters, such as blank spaces available within the transmitted signal and the utilized bandwidth. This paper proposes a learning-based identification framework for heterogeneous signals with orthogonal frequency division multiplexing (OFDM) modulation as generated in a simulated environment at an *a priori* unknown frequency. The implemented region-based signal identification method utilizes cyclostationary features for robust signal detection. Signal characterization is performed using a purposely-built, lightweight, region-based convolutional neural network (R-CNN). It is shown that the proposed framework is robust in the presence of additive white Gaussian noise (AWGN) and, despite its simplicity, shows better performance compared with conventional popular network architectures, such as GoogLeNet, AlexNet, and VGG 16. The signal characterization performance is validated under two degraded environments that are unknown to the system: Doppler shifted and small-scale fading. High performance is demonstrated under both degraded conditions over a wide range of signal to noise ratios (SNRs) and it is shown that the detection probability for the proposed approach is improved over those for conventional energy detectors. It is found that the signal characterization performance deteriorates under extreme conditions, such as lower SNRs and higher Doppler shifts.

INDEX TERMS Blind detection, deep learning, spectrum sensing, cognitive radio, region-based convolutional neural network, software-defined communication, wireless communication.

I. INTRODUCTION

Cognitive communication is a promising solution that can help address the scarcity of spectrum resources in highly dynamic radio frequency (RF) environments for aeronautical wireless communications. Cognitive approaches allow adapting communication parameters following RF environmental changes while sharing the same spectrum between multiple users. Under this paradigm, the secondary users (SUs), those who do not hold frequency licenses, perform signal identification to detect the presence of primary users (PUs) with valid licenses who then access the idle RF spectrum using dynamic spectrum access (DSA) methods. In practice, this not only detects the signals at unknown frequencies, but also characterizes them in both the time and frequency domains. Therefore, this work concerns signal identification rather than simple signal detection, which distinguishes the proposed approach from other works dealing with spectrum sensing.

Spectrum sensing in general is an important function of signal detectors. Multiple algorithms have been proposed for signal detection using energy detection, cyclostationary-based sensing, compressed spectrum sensing, wavelet-based sensing, etc. [1], [2]. It has been shown that cyclostationary properties of communication signals based on their second-order periodicity can be used for signal detection [3]–[5] and its modulation classification [6], [7] using cyclic cross-correlation functions, e.g., using the spectrum coherence function (SCF) [8] or cyclic auto-correlation

The associate editor coordinating the review of this manuscript and approving it for publication was Juan Liu.

function (CAF) [9]. Single-cycle (SCD) or multi-cycle detectors (MCD) [8] can be built using this concept, where the difference between the approaches is in the amount of signal used for processing with a corresponding trade-off between computational complexity and detection efficiency. Implementations of MCD for orthogonal frequency division multiplexing (OFDM) signal detection is discussed in [5] based on the normalized CAFs. Reference [10] proposed an MCD-based fusion of multiple SCDs for time difference of arrival (TDOA) and Doppler shift estimations. Blind SCD using a cyclic correlation function was proposed in [11]. Decision making in such detectors is common by testing binary hypotheses for signal presence [12]–[14] or Markov models (MMs) [4], [15] due to its pattern-matching capability. In the described approaches, the primary challenges are in the variable bias and variance of the SCF and CAF [16], which make it difficult to achieve optimal detection results.

In wireless communications, cyclostationary detection methods commonly assume that the transmission frequency is known to the receiver [6], [17], [18]. Detection, therefore, is typically performed at a particular frequency or within a narrow frequency band of interest. Nevertheless, such an assumption may not be satisfied in wideband sensing scenarios. To address these challenges related frequencies, authors in [19] proposed a wideband sensing solution with a sweeping narrowband detector as characterized with a fixed resolution over the scanning frequency and performed hypothesis testing at each sweeping iteration. Parameter configuration is still a challenge in this case where the performance at low SNRs is affected due to the use of conventional energy detectors. A typical approach to build cyclostationary detectors for wideband scenarios is based on utilizing information from the highest peak in the cyclic domain profile (CDP) [18]. Despite the flexibility offered from this solution, the detection of multiple heterogeneous signals (with respect to their parameters) at adjacent frequencies may be a challenge. Simultaneous detection of multiple heterogeneous signals in [20] was considered using parallel narrowband detectors with signal-specific decision-making policy. This solution brings advantages in terms of the scanning time but requires the careful fusion of decisions from parallel detectors, such as for multi-carrier signals.

Deep learning has attracted significant attention in wireless communication applications as it is model-free and can be used to build flexible end-to-end solutions. For instance, Ref. [21] integrated deep learning in both coding and decoding procedures to form a deep learning aided sparse code multiple access (DL-CDMA) scheme for automatic minimization of the bit error rate (BER). Reference [22] proposed an approach to extract features in the frequency and time domains for blind detection based on the fusion of convolutional neural networks (CNNs) and long short-term memory (LSTM) networks. In [23], a CNN-based module was used to extract Morse signals in a blind wideband sensing scenario. In [24], CNNs were integrated into cooperative spectrum sensing frameworks to improve the sensing accuracy in harsh conditions. References [6], [17] proposed using deep learning approaches, such as CNNs and deep belief networks (DBNs), for RF signal identification and classification based on automatic modulation classification (AMC) schemes.

Region-based convolutional neural networks (R-CNNs) are frequently utilized in a variety of object detection applications due to their good performance when detecting small-scale objects [25], [26]. The detection of arbitrary objects is typically implemented using window shifting [27] with a defined set of extracted features, such as the scale-invariant feature transform (SIFT) [28], histogram of oriented gradient (HOG) [29], or local binary patterns (LBPs) [30]. The drawbacks of such approaches for object detection are related to the lower precision due to the limited information from the feature maps as defined by the low end-to-end efficiency because of manual interventions and the high computational complexity of the shifting window implementation. Also, the problem of parameter identification for communication signals utilized in cognitive radio (CR) frameworks has not received significant attention in the literature.

This paper proposes utilizing a fusion of the cyclostationary detection with a learning-based approach capable of simultaneous detection and characterization of PU transmissions. In this framework both spectrum sensing and signal characterization functionalities are provided for a CR-enabled communication system.

Conventional cyclostationary spectrum sensing relies on *a priori* knowledge of the transmission frequency, which is provided externally in most cases [31]. The proposed spectrum sensing approach operates without such prior signal frequency knowledge. Due to benefits from the fusion of both cyclostationary analysis and the learning-based approach, the proposed method allows extending the spectrum sensing to multiple signal types while simultaneously estimating their frequency, bandwidth, and periodicity and providing robustness in the presence of noise, Doppler shifts, and small-scale fading.

The remainder of this paper is organized as follows: Section II describes the proposed framework, cyclostationary analysis, and designed lightweight R-CNN. The simulations and results are shown in Sec. III, while the analysis and discussions are in Sec. IV. Section V concludes the paper.

II. SPECTRUM IDENTIFICATION FRAMEWORK

The proposed identification approach fuses the cyclostationary detector with the learning-based signal characterization solution. Therefore, there are two distinct parts in the approach architecture: the extraction of cyclostationary features and the characterization of cyclostationary patterns in the signal, as shown in Fig. 1. The solid boxes in the figure represent functions and the dashed boxes are the modules implementing the functions.

In the first stage of the proposed approach, cyclostationary analysis is implemented to convert the signals from the time domain to the frequency-cyclic frequency domain, where

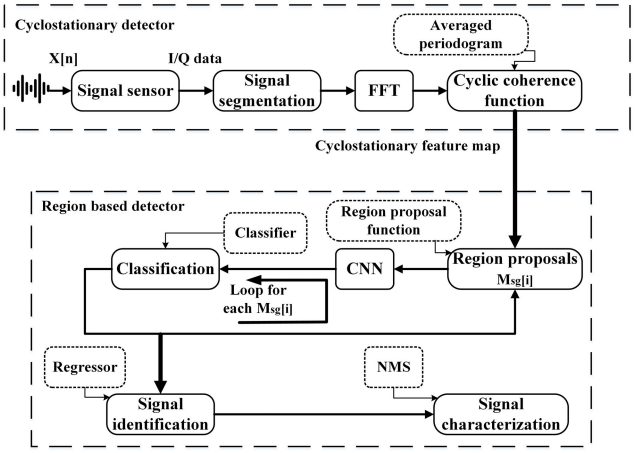

FIGURE 1. Block diagram of the proposed spectrum identification framework.

the spatial and spectral correlations between the frequency components of the signal form the feature map. In the second stage, all available features are extracted from the map using the R-CNN, which is followed by detection and parameter characterization of the PU transmissions. Additional details are given below.

To generate the feature map, the raw data stream $X[n]$ is first split into segments $X_i[n]$ with fixed lengths of n. The feature map is then generated in the frequency-cyclic frequency domain utilizing the fast Fourier transform (FFT) of $X_i[n]$ with the estimated cyclic correlation function from the smoothed periodogram method. This representation of the feature map realizes a simple procedure for communication signal detection, which assumes that signals with no periodic features are presented by wide-sense stationary (WSS) uncorrelated processes [32]. A set of regions of interest (RoI) M_{sg} is then generated in two dimensions after using the region proposal function. Regions with class probabilities over a determined threshold are considered as containing PU transmission. Other regions with the class probabilities below the threshold are removed from the set. Localization of the transmission in the frequency-cyclic frequency domain is performed with a regressor, which extracts the frequency f_c, cyclic frequency f_α, and bandwidth R_c of the PU transmission. The two stages of the framework from Fig. 1 are discussed in more detail.

A. CYCLOSTATIONARY ANALYSIS

A generic instantaneous auto-correlation function for a discrete wideband signal $X[n]$ is defined as [16]:

$$R_X[n,\tau] = \mathbb{E}\left[X[n+(1-\beta)\tau]\cdot X[n-\beta\tau]^*\right] \quad (1)$$

where τ is the time lag, β is a symmetry coefficient, and $(*)$ denotes the complex conjugate operation.

The signal $X[n]$ is considered as cyclostationary with period T_s in a wide sense, when its mean value $\mu_X[n] = \mathbb{E}[X[n]]$ and auto-correlation function R_X are periodic [33]:

$$\mu_X[n] = \mu_X[n+T_s], \quad R_X[n,\tau] = R_X[n+T_s,\tau] \quad (2)$$

When the Fourier series expansion for the auto-correlation function $R_X[n,\tau]$ of the wideband signal $X[n]$ in (1) is convergent [5], it can be presented in the form

$$R_X[n,\tau] = \sum_{\alpha_i\in\mathcal{A}} R_X[\tau;\alpha_i]\, e^{j2\pi\alpha_i n\Delta} \quad (3)$$

where α is the cyclic frequency that belongs to the set $\mathcal{A}$, Δ is the time resolution, and $R_X[\tau;\alpha_i]$ is the Fourier series coefficient given by

$$R_X[\tau;\alpha_i] = \lim_{L\to\infty}\frac{1}{L}\sum_{n=-L/2}^{L/2} R_X[n,\tau]\, e^{-j2\pi\alpha_i n\Delta} \quad (4)$$

The function $R_X[\tau;\alpha_i]$ here is the so-called cyclic auto-correlation function (CAF) [34], where L is the length of the analyzed signal.

The CAF only describes the cyclostationary components in the time domain. For signal characterization in the cyclic frequency domain, the spectral correlation function (SCF) is introduced by performing a Fourier transform (FT) of the CAF [35]: $\Phi_X(f;\alpha) = \mathcal{F}[R_X[\tau;\alpha]]$. The SCF describes the cyclostationary correlations between the spectral components that appear in the signal spectrum with a period characterized by the cyclic frequency $\alpha\in\mathcal{A}$.

Considering that only a finite length signal is available in practical situations, the SCF $\hat{\Phi}_X$ can be estimated using a smoothed cyclic cross-periodogram method [36] as:

$$\hat{\Phi}_X(f;\alpha) = \frac{1}{K\Delta}\sum_{k=0}^{K-1}\mathcal{X}_{n_w}^k[f+(1-\beta)\alpha]\cdot\mathcal{X}_{n_w}^k[f-\beta\alpha]^* \quad (5)$$

where $\mathcal{X}_{n_w}^k$ is the short time Fourier transform (STFT) of $X[n]$, $K = I[(L-n_w)/R]+1$, L is the signal length, n_w is the window width used in the STFT, R is the overlap parameter, and I is a ceiling function that returns the smallest integer value that is greater than or equal to the input value.

The cyclic coherence function (CCF) is another normalized approach to describe the cyclic correlations in the signal spectrum. The CCF $\psi_X(f;\alpha)$ of the signal $X[n]$ is defined as [16]:

$$\psi_X(f;\alpha) = \frac{\mathbb{E}[dX(f+(1-\beta)\alpha)]}{\left\{\mathbb{E}\left[|dX(f+(1-\beta)\alpha)|^2\right]\right\}^{\frac{1}{2}}}\cdot\frac{\mathbb{E}[dX(f-\beta\alpha)]}{\left\{\mathbb{E}\left[|dX(f-\beta\alpha)|^2\right]\right\}^{\frac{1}{2}}} \quad (6)$$

where $dX(f)$ is the spectral increment of X at a frequency f.

Considering the practical limitations on the available signal length, the CCF can be obtained in practice using estimates

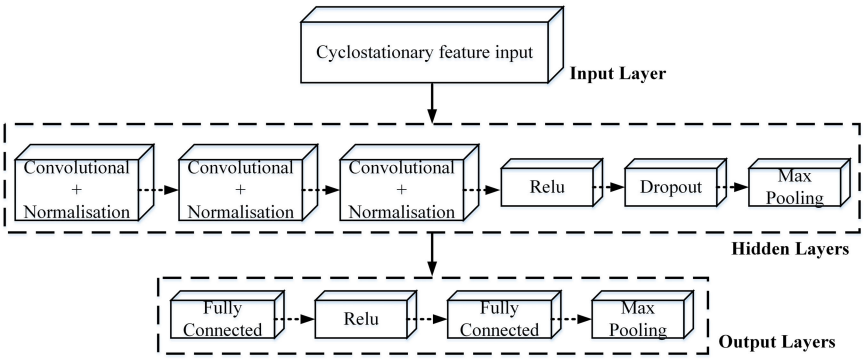

FIGURE 2. Proposed CNN architecture.

for the SCF as obtained from the smoothed cyclic periodogram method (5) as [16]:

$$\hat{\psi}_X(f;\alpha) = \frac{\hat{\Phi}_X(f;\alpha)}{\left\{\hat{\Phi}_X[f+(1-\beta)\alpha;\alpha]\,\hat{\Phi}_X[f-\beta\alpha;\alpha]\right\}^{\frac{1}{2}}}. \quad (7)$$

In contrast to the SCF, the CCF is normalized and more robust due to its lower bias and variance [16]. Therefore, using the CCF is preferred to extract cyclic features in wideband spectrum sensing. In the proposed framework, the CCF represents the feature space that contains generalized information about the communication signals transmitted from PUs. The detection, classification, and characterization of these transmitted signals are performed in the second part of the framework with a region-based detector, as described in the next section.

B. REGION BASED DETECTOR

Detection and classification tasks within the proposed detector are performed using the R-CNN, which can be described in general with the high-level functional diagram in Fig. 3. Detection is performed in two stages. First, the proposed regions are generated, followed by normalization and the application of a CNN to extract feature maps from the re-scaled regions. Second is the classification of regions and locating the detected objects.

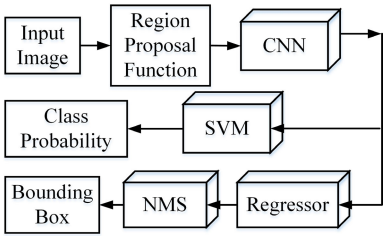

FIGURE 3. Functional diagram of the proposed region-based detector.

Region proposals are performed using a selective search algorithm [37] which generates proposals randomly and then uses complementary similarity measures to combine the regions based on their color, texture, or other factors.

1) LIGHTWEIGHT CONVOLUTIONAL NEURAL NETWORK

The performance of a neural network is highly dependent on several factors, e.g., the types of objects to be detected and classified and the integrity, size, and scale of the training dataset. The design of a neural network usually relies on experience, which makes the adaptation of existing neural network architectures to new applications challenging. Some popular networks, e.g., the GoogLeNet [38], AlexNet [39], and VGG 16 [40], are designed to address the large-scale recognition challenges of complex patterns, where the number of layers is redundant if using them with a small dataset for simple patterns. The above remarks drive the need of having a customized CNN architecture for this case, which results in the proposed lightweight CNN shown in Fig. 2 with the detailed configurations presented in Table 1.

TABLE 1. Configuration of the proposed CNN.

Layer Type	Activations	Learnables
Input layer	300*200*3	N/A
Convolution	296*196*16	Weights (3*3*16), Bias (1*1*16)
Batch normalization	296*196*16	Weights (1*1*16), Scale (1*1*16)
Convolution	292*192*16	Weights (3*3*16*16), Bias (1*1*16)
Batch normalization	292*192*16	Weights (1*1*16), Scale (1*1*16)
Convolution	288*188*16	Weights (3*3*16*16), Bias (1*1*16)
Batch normalization	288*188*16	Weights (1*1*16), Scale (1*1*16)
ReLU	288*188*16	N/A
Dropout	288*188*16	N/A
Max pooling	287*187*16	N/A
Fully connected	1*1*80	Weights (80*858704), Bias (80*1)
ReLU	1*1*80	N/A
Fully connected	1*1*2	Weights (2*80), Bias (2*1)

In contrast to other architectures, the number of activation layers in the proposed CNN is reduced to prevent over-simplification of features due to pre-processing using cyclostationary functions. Fewer pooling layers prevents the dropping of features during processing as the transmission size of the feature map is small compared with the analyzed cyclic frequency and frequency ranges. The stride step of each layer is set to unity to reduce down-sampling issues. Thus, the dropout layer is included to prevent over-fitting considering the small size of the training dataset.

Before feeding the data to the CNN, the data instances are re-scaled to a required size and extended to three dimensions by mapping the normalized cyclic coherence function to the RGB color model. The transformation is implemented primarily for interpretation purposes in the training phase, and the network architecture can be further simplified with a smaller number of activations if such visualization is not needed.

Providing a large number of RoIs after signal identification requires a non-maximum suppression (NMS) layer to reduce their number. This is considered as the engine to decide on fusion [20], which is similar to the case of using "AND" and "OR" rules. This study implements the greedy NMS [41], which is commonly used in many applications [42]. This approach combines regions based on their similarity or distance until no nearby RoIs remain, which demonstrates a good overall performance [41], [42].

2) SIGNAL CHARACTERIZATION

To characterize PU transmissions in terms of the cyclic frequency f_α, frequency f_c, and bandwidth R_c based on the output RoIs (bounding boxes), it is first assumed that all RoIs have a common rectangular format $[x, y, w, h]$, where x and y are the top left corner indices, and w and h are the width and height values of the region, respectively. Considering that the horizontal axis represents the cyclic frequency and the vertical axis is the frequency, the cyclic frequency f_α is obtained as the horizontal center point of the bounding box: $\hat{f_\alpha} = f\{x + w/2\}$ and the estimated frequency $\hat{f_c}$ is obtained from the vertical center point: $\hat{f_c} = f\{y + h/2\}$. The estimated bandwidth of the cyclic coherence feature is the height of the bounding box: $\hat{R_c} = f\{w\}$, where f is the mapping function used to convert the CCF values into the RGB profile as explained in Sec. II-B1.

3) MINIMIZATION FUNCTIONS

We introduce two types of minimization functions here for classification and localization. The minimization function for classification is defined as:

$$argmin_w \sum_i^N max\left(0, 1 - g_i f_w\left(x_i\right)\right) + \lambda \left\|w\right\|^2 \tag{8}$$

where x_i is the instance, g_i is the ground truth for category i ($g_i \in \{0, 1\}$ here), $f_w(x_i)$ is the classifier function, N is the number of proposed regions, $max\left(0, 1 - g_i f_w\left(x_i\right)\right)$ is the standard hinge loss function [43], w is the weight in the classifier, and $\lambda \left\|w\right\|^2$ is the regularization term.

The minimization function for the localization is formulated as a regression problem by minimizing the geometric difference between the ground truth factor t_c and the proposed regions t_b, which have the same rectangular shape as the RoIs, i.e., $[x, y, w, h]$. Therefore, the minimization function (8) can be rewritten as [25]:

$$argmin_{w_2} \sum_i^N \left(t_{c_i} - {w_2}^T \phi\left(t_{b_i}\right)\right)^2 + \lambda \left\|w\right\|^2 \tag{9}$$

where w_2 is the weight in the regressor, $\phi\left(t_{b_i}\right)$ is the feature vector introduced to t_{b_i}, and $\lambda \left\|w_2\right\|^2$ is the regularization term with weight λ.

The ground truth factor t_c is a four-element vector of transformation in terms of the corresponding ground truth t_G defined as:

$$t_{c_x} = \left(t_{G_x} - t_{b_x}\right)/t_{b_w} \tag{10}$$
$$t_{c_y} = \left(t_{G_y} - t_{b_y}\right)/t_{b_h} \tag{11}$$
$$t_{c_w} = log\left(t_{G_w}/t_{b_w}\right) \tag{12}$$
$$t_{c_h} = log\left(t_{G_h}/t_{b_h}\right) \tag{13}$$

4) LOSS FUNCTIONS AND TRAINING PROCEDURE

As a data-driven approach, the R-CNN requires additional training process before being used for detection. Similar to CNN training [44], that for R-CNN is based on a back propagation algorithm using the gradient descend method, where loss functions are required for optimization. The loss function in the regressor can be derived from (9) as: $\mathcal{L}_b = \sum_i^N \left(t_{c_i} - {w_2}^T \phi\left(t_{b_i}\right)\right)^2$. Similarly, the loss function in the classifier can be derived from (8) as: $\mathcal{L}_c = \sum_i^N max\left(0, 1 - y_i f_w\left(x_i\right)\right)$. The loss function for the CNN is defined as $\mathcal{L}_n = \sum_i^M H\left(x_i, \hat{x}_i\right)$, where M is the total number of instances, $\hat{x}$ is the prediction of instance x, and H is the cross-entropy function described in [44]. The total loss $\mathcal{L}$ then defines the combined losses from the classifier, regressor, and training procedure in the CNN and is given as:

$$\mathcal{L} = \mathcal{L}_c/N_c + \lambda_1 \mathcal{L}_b/N_b + \lambda_2 \mathcal{L}_n/N_n \tag{14}$$

where N_c, N_b, and N_n are the numbers of regions used for classification, regression, and CNN training, respectively, and λ_1 and λ_2 are weights for tuning.

The weights are updated in the testing phase after performing back propagation for training. The concept of the update is described using the gradient descend function: $\theta = \theta - W_l \mathcal{J}(\theta)$, where W_l is the learning rate, $\mathcal{J}$ is the gradient descend function, such as based on adaptive moment estimation or stochastic gradient descent [45], and θ is the weight to be updated.

III. EXPERIMENTAL RESULTS

A. SIMULATION SETUP

The OFDM scheme is extensively used in modern communication data links (e.g., IEEE 802.22, LTE, DVB-T/T2, and IEEE 802.11 a/g) due to its remarkable capability to reduce inter-symbol interference (ISI) and multipath effects in air-to-ground communications. Therefore, all the simulation results exploit OFDM symbols to form multi-carrier signals. The ON/OFF process time is employed to simulate PU behavior [46], where "ON" represents the active PU state and "OFF" represents the PU idle state. Therefore, the cyclostationary of simulated signals is induced by the ON/OFF periodicity rather than other cyclostationary features, such as the OFDM cyclic prefix [3].

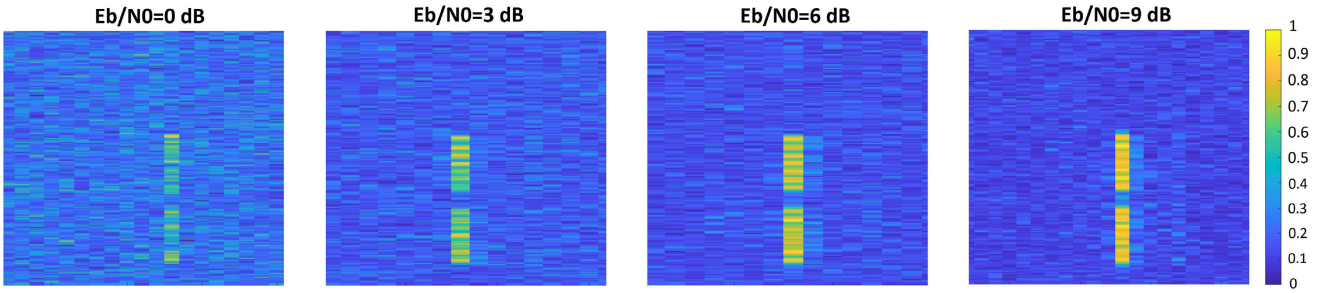

FIGURE 4. Examples of augmented training samples under the AWGN propagation model for different SNRs. Labels on the axes are not shown intentionally as they are not used in the training process.

The simulation of OFDM signals is performed in the GNU Radio environment, which is a powerful toolset to develop software-defined radio applications and corresponding signal processing. The GNU Radio has a graphical user interface, called the GNU Radio Companion (GRC), that makes the development convenient using a block diagram configuration. The block diagram of the signal simulation approach utilizing the ON/OFF model is displayed in Fig. 5.

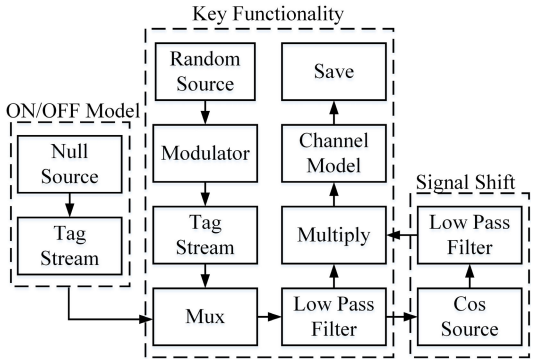

FIGURE 5. Schematic diagram of the OFDM signals simulation using the ON/OFF model.

The random source generates data that are sent to a modulator represented as the ''OFDM Mod'' block. The modulator configuration is set as follows: FFT length of 64 samples, 16 sub-carriers (tones), 32 samples in the cyclic prefix, sampling rate of 44,100 Hz, and BPSK modulation. The modulated signal is then converted into a data stream using the ''tag stream'' module which allows the interleaving of two data streams running in parallel. The ''null source'' module generates blank data segments to simulate the idle PU state in the ON/OFF model. Two data streams are multiplexed into one with the ''Mux'' module according to data tags attached in null signals and modulated signals. Then, the signal is filtered to reduce the interference to other frequencies from sidebands and passed through the channel module, which simulates the propagation environment. The propagation channel is the additive white Gaussian noise (AWGN) model. At the final step, the signal is saved in I/Q format.

B. DATASETS

Two sets of data are required in the experiments for training and testing purposes. To build the training dataset, OFDM signals are simulated by implementing the framework shown in Fig. 5. To introduce more variability in both datasets, randomized data cropping is employed to improve the detection robustness against differences in signal samples and environments. Fig. 4 gives examples of training samples produced by cropping and re-scaling the results of the cyclic coherence functions as applied to the generated OFDM signals.

As mentioned, the training dataset is created using the AWGN model that represents the propagation environment. The SNR values in the AWGN model are selected as $\{-1, -0.5, -0.2, 0, 3, 6, 9\}$ dB.

To demonstrate the region-based cyclostationary detector for PU transmission identification scenarios, a separate dataset is generated by combining multiple OFDM signals that overlap in the frequency domain and with different cyclic frequencies. In addition to the AWGN model used for training, a model with the same parameters is used for the testing data to consider a Doppler shift and small-scale fading environment. The parameters for these environments are presented by a Doppler shift f_d and Rician factor K selected from the values $\{0, 10, 20, 200, 2000\}$ and $\{0, 1, 3, 5, 10\}$, respectively.

For each combination of parameters, 20 records are generated using the simulation model to form samples for the training and testing datasets. As a result, the training data has a total of 140 samples (after re-scaling and cropping), and there are 1,400 samples for testing, which is composed of 700 samples for Doppler shift and 700 samples for environmental fading. The segment length is 1 s, which is determined experimentally to represent the PU signals in the cyclic coherence function. The analysis is performed using a desktop PC with an Intel I7-6700 CPU and 16 GB of RAM.

C. IDENTIFICATION RESULTS

The outputs of the convolutional and fully connected layers are visualized (shown in Fig. 7) to illustrate how the spectrum features are learned by the CNN. During the neural network training, certain similarities are seen by comparing the extracted feature maps in the final layers of Fig. 7 with the original map in Fig. 4, such as the rectangular shape. At the same time, other details, such as tones and gaps between them, are not visible as such features are considered by the CNN to be less important to distinguish signals from the

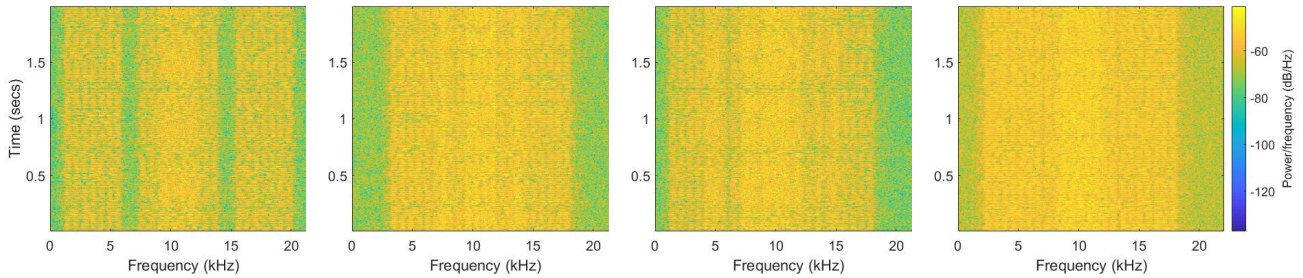

(a) 2 OFDM signals: $f_{\alpha_1} = 88$ Hz, $f_{c_1} = 14$ kHz, $R_{c_1} = 10$ kHz; $f_{\alpha_2} = 90$ Hz, $f_{c_2} = 6$ kHz, $R_{c_2} = 10$ kHz

(b) 2 OFDM signals:$f_{\alpha_1} = 86$ Hz, $f_{c_1} = 11$ kHz, $R_{c_1} = 10$ kHz; $f_{\alpha_2} = 95$ Hz, $f_{c_2} = 7$ kHz, $R_{c_2} = 10$ kHz

(c) 2 OFDM signals:$f_{\alpha_1} = 86$ Hz, $f_{c_1} = 12$ kHz, $R_{c_1} = 10$ kHz; $f_{\alpha_2} = 91$ Hz, $f_{c_2} = 9$ kHz, $R_{c_2} = 10$ kHz

(d) 3 OFDM signals:$f_{\alpha_1} = 86$ Hz, $f_{c_1} = 7$ kHz, $R_{c_1} = 10$ kHz; $f_{\alpha_2} = 88$ Hz, $f_{c_2} = 9$ kHz, $R_{c_2} = 10$ kHz; $f_{\alpha_3} = 90$ Hz, $f_{c_3} = 12$ kHz, $R_{c_3} = 10$ kHz

FIGURE 6. Spectrograms of multiple OFDM signals for $Eb/N0 = 6$ dB.

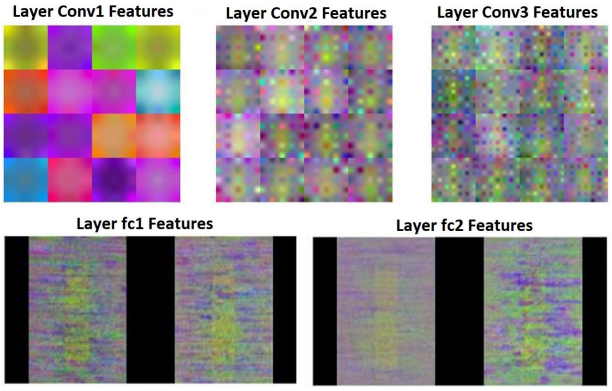

FIGURE 7. Visualization of layers in the CNN (better details are seen when viewed in color).

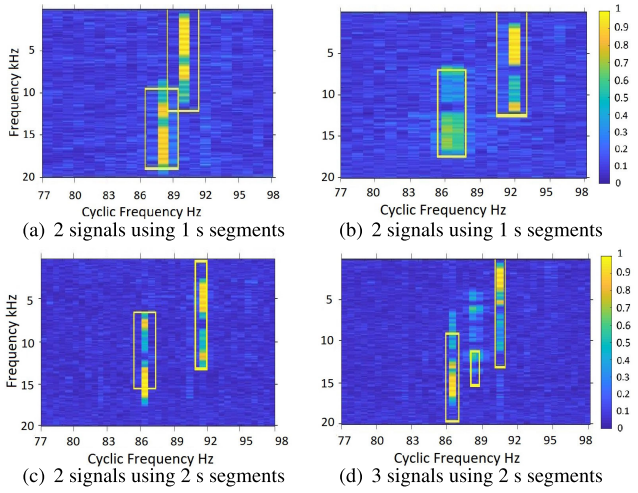

(a) 2 signals using 1 s segments

(b) 2 signals using 1 s segments

(c) 2 signals using 2 s segments

(d) 3 signals using 2 s segments

FIGURE 8. Region-based cyclostationary identification of multiple OFDM signals at $Eb/N0 = 6$ dB.

background. It is seen that the noise in the final layers is emphasized more due to a significant proportion of training samples that are severely affected by the AWGN environment.

To demonstrate the capabilities of the proposed approach in multi-signal identification, a separate dataset was generated consisting of four groups of data with multiple OFDM signals at neighboring frequencies f_c and variable f_α and R_c. The spectrograms of these signals are shown in Fig. 6. It is seen that the signals overlap in the frequency domain, making it challenging to detect and recognize such signals using conventional approaches. Multi-signal detection with the proposed approach is illustrated in Fig. 8, where the detected signals are presented with rectangles (bounding boxes) that are used to characterize the signal parameters. It is seen that the signals processed with the proposed identification approach are well separated and their parameters can be easily estimated using the bounding box positions and dimensions.

It is seen from Fig. 8 that each signal with cyclic behavior is fully or partially enclosed within a bounding box. The bounding boxes are successfully generated for signals with fluctuating magnitudes and distorted shapes in the cyclic coherence feature space (see the left feature in Fig. 8(b)). This behavior confirms the reliability of the proposed approach against variability in signal characteristics. Furthermore, utilizing longer data segments (duration of 2 s instead of 1 s) improves both the resolution and level of noise in the feature space and provides a means for better identification.

By observing the simultaneous identification of the three signals in Fig. 8(d), the identification at low magnitudes and distorted cyclic features is a challenge when other stronger signals exist. Detection of these signals using conventional methods, where only the maximum value of spectrum profile is analyzed, is not possible, which further excludes parameter identification. The proposed learning-based approach has the advantage here due to the consideration of more features, such as the signal shape in the cyclic frequency domain and correlations between subcarriers. Therefore, the qualitative comparison shows that the proposed spectrum identification framework can simultaneously identify multiple heterogeneous signals (in terms of their modulation parameters) while traditional methods cannot.

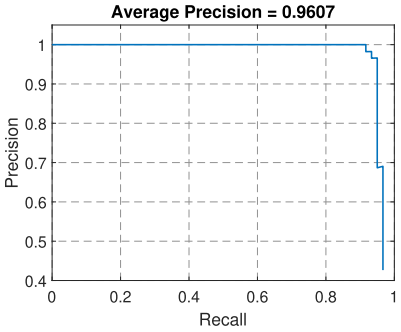

FIGURE 9. Precision-recall curve for the proposed identification framework in the training phase.

IV. ANALYSIS AND DISCUSSION

To quantitatively evaluate the performance of the proposed region-based detector, the training and testing phases are analyzed separately. A comparison with other well-known neural networks, such as AlexNet, GoogLeNet, and VGG 16, is given for the training phase. In the testing phase, the influence of unknown propagation models on the detector performance is evaluated.

1) TRAINING PHASE PERFORMANCE ANALYSIS

Signal classification performance of the proposed detector is analyzed using the precision-recall (PR) curve. Precision describes the retrieval ratio between the relevant instances and recall describes the retrieval ratio between the full set of instances [47], [48]. The distance (relevance) measurement is realized through analyzing the overlap ratio between regions based on the intersection over union (IoU) definition [41] with a threshold of 0.5. The average precision (AP) is calculated to measure the recall and precision for the ranked retrieval results. The calculated PR curve and corresponding AP value are shown in Fig. 9 based on the hyper-parameter values shown in Table. 2.

TABLE 2. Configuration values of the hyper-parameters.

Hyper-parameter	Specification
Batch size	40
Epoch size	20
Initial learning rate	0.0001
Negative overlap range	$[0.1, 0.3]$
Positive overlap range	$[0.5, 1]$
Number of strongest regions	1000

It is seen from Fig. 9 that the precision remains at 100% until the recall value reaches 0.92. A large area below the PR curve verifies the outstanding performance of the proposed approach compared with other object detection applications [49]. This result is also confirmed from the high AP of 0.9607. Therefore, the training performance analysis using both the PR curve and AP confirms success in developing a lightweight neural network and in the selection of an effective hyper-parameter configuration for signal identification.

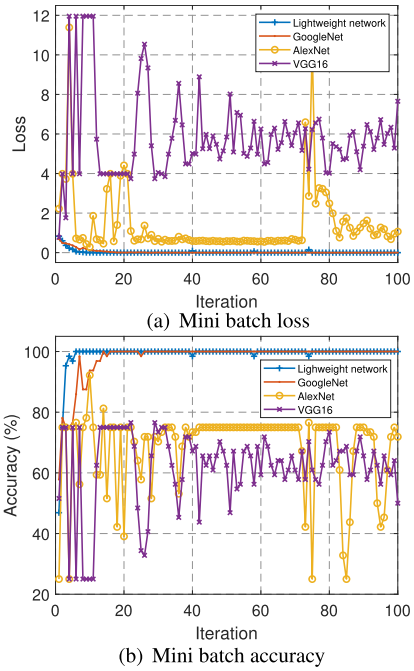

FIGURE 10. Comparison of loss and accuracy for popular deep neural networks.

As a comparison, the performance of the proposed lightweight neural network, AlexNet, GoogLeNet, and VGG 16 are analyzed. The compared metrics are the time consumption, loss as defined by Eq. (14), and accuracy, where the latter represents multiple successful detections for the entire training dataset when the IoU for the bounding box and ground truth exceeds 0.5. The same hyper-parameter configuration as shown in Table. 2 is used at this stage. The results for the time consumption as compared with other common networks are shown in Table. 3.

TABLE 3. Training time comparison between popular deep neural networks.

Network	Proposed	GoogLeNet	AlexNet	VGG 16
Time (hh:mm:ss)	00:04:26	00:19:45	00:13:29	01:30:25

An analysis of the results in Table. 3 shows that the VGG 16 has the longest training time at more than 18 times that for the proposed lightweight network. The results also show that GoogLeNet and AlexNet are faster than the VGG 16 in the training phase, but still slower than the proposed network by factors of 3 and 2, respectively.

The loss and accuracy results in the training phase are shown in Fig. 10. The VGG 16 is not only the slowest network for the training phase, but also has the worst performance in terms of accuracy and loss between the considered networks. The performance of the AlexNet is better than the VGG 16 with a final accuracy fluctuating around 75% and a loss value of 1. The GoogLeNet presents similar results to the proposed lightweight network performance in terms of

the steady-state values of loss and accuracy, which converge to 0 and 100%, respectively.

It is noted that the rate of convergence for the GoogLeNet is lower than that for the proposed network, which highlights its advantage in this area. It is also noted that spikes in the results of the proposed network are caused by a dropout function and can be ignored in the analysis.

Therefore, it is concluded that the performance of the proposed network is an improvement over conventional networks for the considered case of multiple-signal detection and characterization.

2) DETECTOR PERFORMANCE IN UNKNOWN ENVIRONMENTS

As the performance of a detector is determined to a significant extent by the channel model during training, the impact of the unknown channel model on the performance of the proposed identification approach is analyzed. The Doppler shift f_d and Rician fading with factor K are introduced to simulate realistic propagation effects. The assessment concerns two aspects of the identification process: confidence and precision measurements.

The averaged confidence score is calculated for each successful detection in the testing dataset following a common approach described in [50] in the form of a normalized strength of the most activated unit in the output layer of the neural network. The equation is formulated as $\sum_{i=1}^{N} \frac{\overline{e^z}}{\sum_{i=1}^{K} e_i^z}$, where e is the exponential function, K is the category number, z is the strength of the activated unit trained with the dataset, and N is the number of samples that are detected successfully. It is noted that in contrast to detection-oriented approaches, e.g., [18], this work considers performance measurements and optimization in terms of errors in the estimated signal parameters; therefore, the probability of correct diagnostics is not calculated directly. The resulting confidence scores are shown in Fig. 11.

Observing the trends in the curves for both the Doppler shift and Rician fading effects shows that the proposed detector has a high confidence (over 74% at relatively low SNRs) under both unknown conditions.

The identification confidence increases for larger $Eb/N0$ from -1 to 6 dB. However, starting from 6 dB, the confidence score may decrease in some cases. Such abnormal behavior is explained by the imbalanced nature of the training dataset. Based on the visualization results for the output layer in Fig. 7, the learned pattern is surrounded by noise. When $Eb/N0 > 6$ dB the noise becomes barely noticeable compared with the signal-related features. Therefore, the detector may treat this condition as not belonging to a known class.

It is also seen from Fig. 7 that there is a correlation between the Doppler shift f_d and the confidence score. Typically, a higher confidence corresponds to results obtained at lower Doppler shifts due to smaller distortions in the signal spectral and cyclic characteristics. However, such relationships are not apparent when Rician fading is present. This can be explained by the random nature of fading, which has a limited impact on the spectral characteristics of signals.

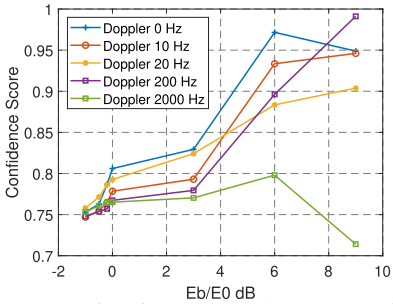

(a) Change of confidence score with Doppler shift f_d

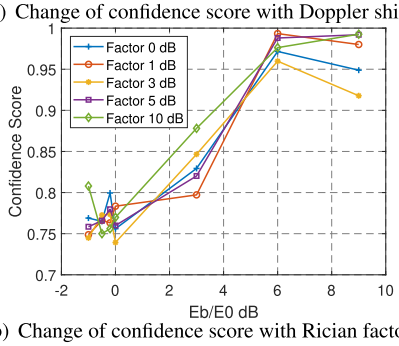

(b) Change of confidence score with Rician factor K

FIGURE 11. Confidence scores in unknown environments.

The detection probabilities for the proposed approach are compared with the energy detection approach, which utilizes the constant false alarm rate (CFAR) method [51], with the data for an AWGN environment to benchmark the performance. As the proposed method does not have a dedicated detection stage, the detection probability is derived indirectly from the confidence scores. The detection decisions are made when the confidence score exceeds 0.7 following the approach proposed in [52]. The comparison results are shown in Table 4. The proposed approach has a higher detection efficiency at lower SNRs compared with the energy detector. It is noted that the signal characterization, such as the extraction of the PU signal frequency and bandwidth, offered by the proposed approach is a challenge for the conventional energy detector.

TABLE 4. Probability of detection in an AWGN environment.

Eb/N0 (dB)	-4	-2	-1	-0.5	0	3	6	9
Energy detection	0	0	0	0.01	0.26	0.99	1	1
Learning based detection	0.3	0.65	0.85	0.95	0.95	0.95	1	0.95

It is seen from the results that the performance of the utilized energy detector is not the same as those presented in other papers [53], [54]. We attribute this variability to two factors: differences in the analysis parameters and differences in the actual SNRs of the signal. The $Eb/N0$ ratio is used to characterize the noise rather than the conventional SNR measures due to known challenges of defining the SNR for OFDM signals. Overall, the results shown in Fig. 11 indicate

the proposed approach has a detection performance that is similar to other cyclostationary detectors, such as those utilized in other works [53], [54].

To demonstrate the performance of signal parameter estimation, the measure L is formulated using the mean square error (MSE). It is commonly accepted [55] that MSE-based measures are suitable to characterize precision and accuracy as they combine both bias and variance of the investigated parameter. The implemented measure accounts for the MSE-based contributions from key signal parameters as extracted from the proposed approach, i.e., cyclic frequency $\hat{f}_\alpha$, frequency $\hat{f}_c$, and bandwidth $\hat{R}_c$:

$$L = \sum_{i=1}^{N} \frac{\overline{\frac{\hat{f}_{\alpha i} - f_\alpha}{f_\alpha}}^2 + \overline{\frac{\hat{f}_{ci} - f_c}{f_c}}^2 + \overline{\frac{\hat{R}_{ci} - R_c}{R_c}}^2}{N} \tag{15}$$

where N is the number of samples, f_α, f_c, and R_c are the true values for the cyclic frequency, frequency, and bandwidth, respectively, and the overbar denotes the averaged estimated value.

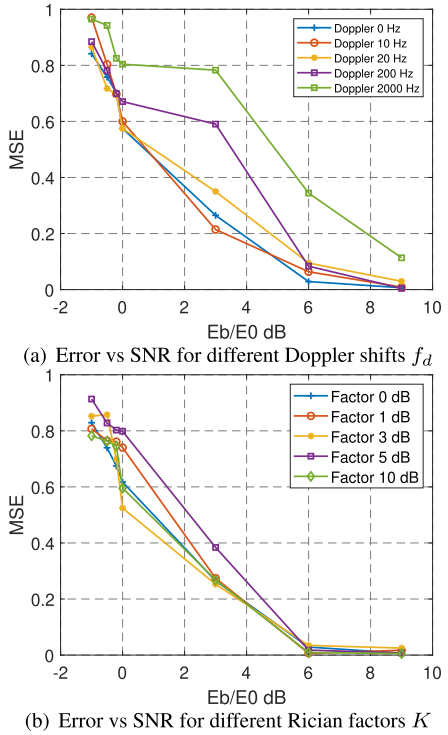

(a) Error vs SNR for different Doppler shifts f_d

(b) Error vs SNR for different Rician factors K

FIGURE 12. Dependency of the error measure (15) on the SNR for testing under degraded environment conditions.

It is seen from Fig. 12 that the measure defined in (15) decreases when the noise levels reduce and typically converges to below 0.1 within the $Eb/N0$ range of $[-1, 6]$ dB. This indicates that the proposed method demonstrates a high parameter characterization performance (in the MSE sense) when the SNR is above 6 dB, even in the worst case of a Doppler shift of 2000 Hz. When the conditions are more relaxed, i.e., lower Doppler shifts and any considered Rician factor, the proposed method shows the same high performance starting from a 3-dB SNR. This behavior is similar to that for the confidence dependencies in Fig. 11; the increased Doppler shift f_d reduces the detector performance, which is not observed in case of Rician fading.

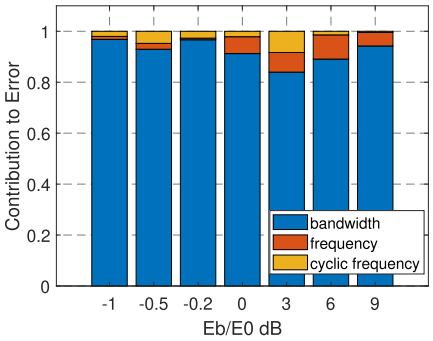

FIGURE 13. Error composition for the worst case Doppler shift of $f_d = 2000$ Hz.

To provide more details on individual error contributions from each parameter, the curve with the highest error was selected from Fig. 12, which corresponds to a Doppler shift of $f_d = 2000$ Hz, to create the composition chart in Fig. 13. The errors displayed for f_α, f_c, and R_c are shown separately. The results indicate that the largest contribution to the overall error is from the bandwidth identification (blue bars), as the estimated bandwidth is always wider than the actual value due to noise and leakage effects. This error is followed by a much smaller error in the frequency identification (red bars), which is on average below 5%. The smallest contributor is the error in cyclic frequency (orange bars). It can be seen that in the worst case (corresponding to and $Eb/N0$ of 3 dB) where the MSE error measure L reaches 0.8 in Fig. 12, individual errors in the cyclic frequency and frequency are relatively low at approximately 0.05. The other noise-level errors decrease. The main reason for the larger bandwidth estimation error is in the way information is handled from multiple bounding boxes, which causes overestimation. Therefore, the detector can identify the cyclic frequency and frequency more precisely, while the bandwidth estimation requires further improvement.

V. CONCLUSION

This paper proposes a spectrum identification framework for signal characterization in cognitive radio applications with unknown communication frequency. It integrates cyclostationary feature maps with cyclic coherence function and characterizes parameters of cyclic frequency, frequency and bandwidth by implementing a region-based identification approach.

It has been found that the proposed framework shows a well performance under degraded environment conditions that were not included in the training dataset - Doppler shifts and small-scale fading. The performance tested down to -1 dB $Eb/N0$ has shown a high confidence score of 74% for

the worst case. The MSE converges to below 0.1 for $Eb/N0$ above 6 dB. To benchmark the detection performance of the proposed method, we estimate detection probabilities and compare them with energy detection results. Our approach allows extension of usable SNRs towards lower values by approximately 3 dB. At the same time our approach allows signal parameter's characterization, which is not offered by other techniques and is more challenging when energy detectors are used, especially among multi-carrier signals.

The designed lightweight neural network utilized in the proposed framework has shown its high efficiency compared with other popular networks, such as GoogLeNet, AlexNet and VGG 16 in terms of better training performance and faster training speed.

Future work will be focused on a deeper analysis of the performance at low SNRs, further parameter optimization and study of requirements and measures of the training data quality. These improvements will open up many other applications with the proposed solution, such as the identification of RF fingerprints and specific emitter signals.

REFERENCES

[1] Y. Zeng, Y.-C. Liang, A. T. Hoang, and R. Zhang, "A review on spectrum sensing for cognitive radio: Challenges and solutions," *EURASIP J. Adv. Signal Process.*, vol. 2010, no. 1, pp. 1–15, Dec. 2010.
[2] T. Yucek and H. Arslan, "A survey of spectrum sensing algorithms for cognitive radio applications," *IEEE Commun. Surveys Tuts.*, vol. 11, no. 1, pp. 116–130, 1st Quart., 2009.
[3] A. Punchihewa, O. A. Dobre, S. Rajan, and R. Inkol, "Cyclostationarity-based algorithm for blind recognition of OFDM and single carrier linear digital modulations," in *Proc. IEEE 18th Int. Symp. Pers., Indoor Mobile Radio Commun.*, Sep. 2007, pp. 1–5.
[4] K. Kim, I. A. Akbar, K. K. Bae, J.-S. Um, C. M. Spooner, and J. H. Reed, "Cyclostationary approaches to signal detection and classification in cognitive radio," in *Proc. 2nd IEEE Int. Symp. New Frontiers Dyn. Spectr. Access Netw.*, Apr. 2007, pp. 212–215.
[5] T. E. Bogale and L. Vandendorpe, "Multi-cycle cyclostationary based spectrum sensing algorithm for OFDM signals with noise uncertainty in cognitive radio networks," in *Proc. IEEE Mil. Commun. Conf. (MILCOM)*, Oct. 2012, pp. 1–6.
[6] G. J. Mendis, J. Wei-Kocsis, and A. Madanayake, "Deep learning based radio-signal identification with hardware design," *IEEE Trans. Aerosp. Electron. Syst.*, vol. 55, no. 5, pp. 2516–2531, Oct. 2019.
[7] E. E. Azzouz and A. K. Nandi, *Automatic Modulation Recognition of Communication Signals*. Norwell, MA, USA: Kluwer, 1996.
[8] A. Ivanov, A. Mihovska, K. Tonchev, and V. Poulkov, "Real-time adaptive spectrum sensing for cyclostationary and energy detectors," *IEEE Aerosp. Electron. Syst. Mag.*, vol. 33, nos. 5–6, pp. 20–33, May 2018.
[9] A. Tani, R. Fantacci, and D. Marabissi, "A low-complexity cyclostationary spectrum sensing for interference avoidance in femtocell LTE-A-based networks," *IEEE Trans. Veh. Technol.*, vol. 65, no. 4, pp. 2747–2753, Apr. 2016.
[10] Z. Huang, Y. Zhou, and W. Jiang, "TDOA and Doppler estimation for cyclostationary sgnals based on multi-cycle frequencies," *IEEE Trans. Aerosp. Electron. Syst.*, vol. 44, no. 4, pp. 1251–1264, Oct. 2008.
[11] K. Kosmowski, M. Suchański, J. Pawelec, and M. Kustra, "A novel OFDM sensing method based on CAF-max for hybrid detectors architecture," in *Proc. Int. Conf. Mil. Commun. Inf. Syst. (ICMCIS)*, May 2016, pp. 1–4.
[12] R. I. C. Chiang, G. B. Rowe, and K. W. Sowerby, "A quantitative analysis of spectral occupancy measurements for cognitive radio," in *Proc. IEEE 65th Veh. Technol. Conf. (VTC-Spring)*, Apr. 2007, pp. 3016–3020.
[13] D. Sun, T. Song, B. Gu, X. Li, J. Hu, and M. Liu, "Spectrum sensing and the utilization of spectrum opportunity tradeoff in cognitive radio network," *IEEE Commun. Lett.*, vol. 20, no. 12, pp. 2442–2445, Dec. 2016.
[14] O. A. Y. Ojeda and J. Grajal, "Sensitivity analysis of cyclostationarity-based and radiometric detectors for single-sensor receivers," *IEEE Trans. Aerosp. Electron. Syst.*, vol. 48, no. 1, pp. 27–43, Jan. 2012.
[15] C. Ghosh, C. Cordeiro, D. P. Agrawal, and M. B. Rao, "Markov chain existence and hidden Markov models in spectrum sensing," in *Proc. IEEE Int. Conf. Pervas. Comput. Commun.*, Mar. 2009, pp. 1–6.
[16] J. Antoni, "Cyclic spectral analysis in practice," *Mech. Syst. Signal Process.*, vol. 21, no. 2, pp. 597–630, Feb. 2007. [Online]. Available: http://www.sciencedirect.com/science/article/pii/S0888327006001816
[17] Z. Xu, A. Savvaris, A. Tsourdos, and T. Alawadi, "High-frequency band automatic mode recognition using deep learning," in *Proc. IEEE/AIAA 37th Digit. Avionics Syst. Conf. (DASC)*, Sep. 2018, pp. 1–5.
[18] D. B. Rawat, "Evaluating performance of cognitive radio users in MIMO-OFDM-based wireless networks," *IEEE Wireless Commun. Lett.*, vol. 5, no. 5, pp. 476–479, Oct. 2016.
[19] D. Pfammatter, D. Giustiniano, and V. Lenders, "A software-defined sensor architecture for large-scale wideband spectrum monitoring," in *Proc. 14th Int. Conf. Inf. Process. Sensor Netw. (IPSN)*. New York, NY, USA: Association for Computing Machinery, 2015, pp. 71–82, doi: 10.1145/2737095.2737119.
[20] O. Olabiyi and A. Annamalai, "Parallel multi-channel detection: A practical solution to energy detection of heterogeneous wideband spectrum," in *Proc. 35th IEEE Sarnoff Symp.*, May 2012, pp. 1–5.
[21] M. Kim, N.-I. Kim, W. Lee, and D.-H. Cho, "Deep learning-aided SCMA," *IEEE Commun. Lett.*, vol. 22, no. 4, pp. 720–723, Apr. 2018.
[22] D. Ke, Z. Huang, X. Wang, and X. Li, "Blind detection techniques for non-cooperative communication signals based on deep learning," *IEEE Access*, vol. 7, pp. 89218–89225, 2019.
[23] Y. Yuan, Z. Sun, Z. Wei, and K. Jia, "DeepMorse: A deep convolutional learning method for blind morse signal detection in wideband wireless spectrum," *IEEE Access*, vol. 7, pp. 80577–80587, 2019.
[24] W. Lee, M. Kim, and D.-H. Cho, "Deep cooperative sensing: Cooperative spectrum sensing based on convolutional neural networks," *IEEE Trans. Veh. Technol.*, vol. 68, no. 3, pp. 3005–3009, Mar. 2019.
[25] R. Girshick, J. Donahue, T. Darrell, and J. Malik, "Rich feature hierarchies for accurate object detection and semantic segmentation," in *Proc. IEEE Conf. Comput. Vis. Pattern Recognit.*, Jun. 2014, pp. 580–587.
[26] C. Zhang, X. Xu, and D. Tu, "Face detection using improved faster RCNN," 2018, *arXiv:1802.02142*. [Online]. Available: http://arxiv.org/abs/1802.02142
[27] R. Vaillant, C. Monrocq, and Y. L. Cun, "Original approach for the localisation of objects in images," *IEE Proc.-Vis., Image Signal Process.*, vol. 141, no. 4, pp. 245–250, Aug. 1994.
[28] D. G. Lowe, "Distinctive image features from scale-invariant keypoints," *Int. J. Comput. Vis.*, vol. 60, no. 2, pp. 91–110, Nov. 2004.
[29] N. Dalal and B. Triggs, "Histograms of oriented gradients for human detection," in *Proc. IEEE Comput. Soc. Conf. Comput. Vis. Pattern Recognit. (CVPR)*, vol. 1, Jun. 2005, pp. 886–893.
[30] T. Ojala, M. Pietikainen, and T. Maenpaa, "Multiresolution gray-scale and rotation invariant texture classification with local binary patterns," *IEEE Trans. Pattern Anal. Mach. Intell.*, vol. 24, no. 7, pp. 971–987, Jul. 2002.
[31] S. Pandit and G. Singh, *Spectrum Sharing in Cognitive Radio Networks*. Berlin, Germany: Springer, 2017.
[32] P. Vijayakumar, J. George, S. Malarvizhi, and A. Sriram, "Analysis and implementation of reliable spectrum sensing in OFDM based cognitive radio," in *Smart Computing and Informatics*. Singapore: Springer, 2018, pp. 565–572.
[33] W. A. Gardner, A. Napolitano, and L. Paura, "Cyclostationarity: Half a century of research," *Signal Process.*, vol. 86, no. 4, pp. 639–697, Apr. 2006.
[34] W. A. Gardner, *Statistical Spectral Analysis: A Nonprobabilistic Theory*. Upper Saddle River, NJ, USA: Prentice-Hall, 1986.
[35] I. G. Anyim, J. Chiverton, M. Filip, and A. Tawfik, "Efficient and low complexity optimized feature spectrum sensing with receiver offsets," in *Proc. IEEE Wireless Commun. Netw. Conf. (WCNC)*, Apr. 2018, pp. 1–6.
[36] R. S. Roberts, W. A. Brown, and H. H. Loomis, "Computationally efficient algorithms for cyclic spectral analysis," *IEEE Signal Process. Mag.*, vol. 8, no. 2, pp. 38–49, Apr. 1991.
[37] J. R. R. Uijlings, K. E. A. van de Sande, T. Gevers, and A. W. M. Smeulders, "Selective search for object recognition," *Int. J. Comput. Vis.*, vol. 104, no. 2, pp. 154–171, Sep. 2013.
[38] C. Szegedy, W. Liu, Y. Jia, P. Sermanet, S. Reed, D. Anguelov, D. Erhan, V. Vanhoucke, and A. Rabinovich, "Going deeper with convolutions," in *Proc. Comput. Vis. Pattern Recognit. (CVPR)*, Jun. 2015, pp. 1–9. [Online]. Available: http://arxiv.org/abs/1409.4842
[39] A. Krizhevsky, I. Sutskever, and G. E. Hinton, "ImageNet classification with deep convolutional neural networks," in *Proc. Adv. Neural Inf. Process. Syst.*, 2012, pp. 1097–1105.

[40] K. Simonyan and A. Zisserman, "Very deep convolutional networks for large-scale image recognition," 2014, *arXiv:1409.1556*. [Online]. Available: http://arxiv.org/abs/1409.1556
[41] A. Neubeck and L. Van Gool, "Efficient non-maximum suppression," in *Proc. 18th Int. Conf. Pattern Recognit. (ICPR)*, vol. 3, 2006, pp. 850–855.
[42] R. Rothe, M. Guillaumin, and L. Van Gool, "Non-maximum suppression for object detection by passing messages between windows," in *Proc. Asian Conf. Comput. Vis.* Cham, Switzerland: Springer, 2014, pp. 290–306.
[43] P. L. Bartlett and M. H. Wegkamp, "Classification with a reject option using a hinge loss," *J. Mach. Learn. Res.*, vol. 9, pp. 1823–1840, Aug. 2008.
[44] I. Goodfellow, Y. Bengio, and A. Courville, *Deep Learning*. Cambridge, MA, USA: MIT Press, 2016.
[45] D. P. Kingma and J. Ba, "Adam: A method for stochastic optimization," 2014, *arXiv:1412.6980*. [Online]. Available: http://arxiv.org/abs/1412.6980
[46] S. Geirhofer, L. Tong, and B. M. Sadler, "Cognitive radios for dynamic spectrum access-dynamic spectrum access in the time domain: Modeling and exploiting white space," *IEEE Commun. Mag.*, vol. 45, no. 5, pp. 66–72, 2007.
[47] H. Müller, W. Müller, D. M. Squire, S. Marchand-Maillet, and T. Pun, "Performance evaluation in content-based image retrieval: Overview and proposals," *Pattern Recognit. Lett.*, vol. 22, no. 5, pp. 593–601, Apr. 2001.
[48] L. Liu and M. T. Özsu, *Encyclopedia of Database Systems*, vol. 6. New York, NY, USA: Springer, 2009.
[49] Y. Zhu, R. Urtasun, R. Salakhutdinov, and S. Fidler, "SegDeepM: Exploiting segmentation and context in deep neural networks for object detection," in *Proc. IEEE Conf. Comput. Vis. Pattern Recognit. (CVPR)*, Jun. 2015, pp. 4703–4711.
[50] A. Mandelbaum and D. Weinshall, "Distance-based confidence score for neural network classifiers," 2017, *arXiv:1709.09844*. [Online]. Available: http://arxiv.org/abs/1709.09844
[51] D. M. M. Plata and Á. G. A. Reátiga, "Evaluation of energy detection for spectrum sensing based on the dynamic selection of detection-threshold," *Procedia Eng.*, vol. 35, pp. 135–143, Jan. 2012.
[52] Q. Fang, H. Li, X. Luo, L. Ding, H. Luo, T. M. Rose, and W. An, "Detecting non-hardhat-use by a deep learning method from far-field surveillance videos," *Autom. Construct.*, vol. 85, pp. 1–9, Jan. 2018. [Online]. Available: http://www.sciencedirect.com/science/article/pii/S0926580517304429
[53] A. Nafkha, M. Naoues, K. Cichon, and A. Kliks, "Experimental spectrum sensing measurements using USRP software radio platform and GNU-radio," in *Proc. 9th Int. Conf. Cognit. Radio Oriented Wireless Netw. (CROWNCOM)*, 2014, pp. 429–434.
[54] S. H. Sohn, N. Han, J. M. Kim, and J. W. Kim, "OFDM signal sensing method based on cyclostationary detection," in *Proc. 2nd Int. Conf. Cognit. Radio Oriented Wireless Netw. Commun.*, Aug. 2007, pp. 63–68.
[55] A. den Dekker and J. Sijbers, "Estimation of signal and noise parameters from MR data," in *Advanced Image Processing in Magnetic Resonance Imaging*, vol. 27. Boca Raton, FL, USA: CRC Press, 2005, pp. 85–143.

ZHENGJIA XU (Graduate Student Member, IEEE) received the B.S. degree in civil aviation electrical and electronic engineering and the M.S. degree in vehicle operation engineering from the Nanjing University of Aeronautics and Astronautics, Nanjing, China, in 2014 and 2017, respectively. He is currently pursuing the Ph.D. degree with Cranfield University. His current research interests include cognitive communications for UAV applications, such as signal identification (deep learning approaches), spectrum allocation, cognitive communications, and UAV communication architecture.

IVAN PETRUNIN (Member, IEEE) received the M.Sc. degree in design and manufacturing of electronic equipment from the National Technical University of Ukraine, in 1998, and the Ph.D. degree in signal processing for condition monitoring from Cranfield University, U.K., in 2013.

He is currently a Lecturer in digital signal processing with the Centre for Autonomous and Cyber-Physical Systems, Cranfield University. His current research interests include applied signal processing for autonomous systems with particular emphasis on communications, navigation, and surveillance aspects, such as cognitive communication schemes, assured multisensor navigation, and remote sensing.

ANTONIOS TSOURDOS (Member, IEEE) received the M.Eng. degree in electronic, control, and systems engineering from The University of Sheffield, Sheffield, U.K., in 1995, the M.Sc. degree in systems engineering from Cardiff University, Cardiff, U.K., in 1996, and the Ph.D. degree in nonlinear robust missile autopilot design and analysis from Cranfield University, Cranfield, U.K., in 1999.

He was the Head of the Autonomous Systems Group, Cranfield University, in 2007, where he is currently a Professor of control systems. He was also involved with SEAS DTC on Autonomous Systems Verifications. He has published over 100 peer-reviewed journal and conference papers. His research interests include guidance and control of single and multiple vehicles, and the verifiable autonomy of autonomous systems with a recent focus on the new important subjects of integrated system health management and cyber-physical systems.

Dr. Tsourdos was a member of the Team Stellar, U.K. MoD Grand Challenge, in 2008. He is a member of the IFAC Technical Committee on Intelligent Autonomous Vehicles, the IET Executive Team on Robotics and Automation, and the ATI Autonomous Systems National Technical Committee. He received the IET Innovation Award, Category Team, in 2009. He is also an editorial board member on several international publications, including IMechE and the IEEE.